

Supporting Information

Ultrathin Perovskite Derived Ir-Based Nanosheets for High-Performance Electrocatalytic Water Splitting

Shangheng Liu,^{a,b,‡} Yingtian Zhang,^{c,‡} Xinnan Mao,^{d,e,‡} Ling Li,^b Ying Zhang,^a Leigang Li,^a Yu Pan,^c Xingang Li,^c Lu Wang,^{e,*}, Qi Shao,^b Yong Xu,^{d,*} and Xiaoqing Huang^{a,*}

E-mail: lwang22@suda.edu.cn, yongxu@gdut.edu.cn, hxq006@xmu.edu.cn

Experimental Section

1.1 Chemicals. Hydrogen hexachloroiridate (IV) hexahydrate ($\text{H}_2\text{IrCl}_6 \cdot \text{H}_2\text{O}$, 99%) and commercial IrO_x were obtained from Alfa Aesar. Tetramethylammonium hydroxide ($(\text{CH}_3)_4\text{NOH}$, 99%) was obtained from Energy Chemical. Zinc chloride (II) (ZnCl_2 , 98%), sodium hydroxide (NaOH , 96%), potassium hydroxide (KOH , 85%) and ethanol ($\text{C}_2\text{H}_5\text{OH}$, 99.7%) were obtained from Sinopharm Chemical Reagent Co. Ltd. Nafion solution (~5 wt.% in a mixture of lower aliphatic alcohols and water) was obtained from Sigma-Aldrich. The commercial Ir/C (20 wt% loading) was obtained from Premetek Co. The commercial Pt/C (20 wt% loading) and carbon powder (XC72R) were purchased from Johnson Matthey (JM) and Vulcan, respectively. The deionized water ($18 \text{ M}\Omega \text{ cm}^{-1}$) used in all experiments was prepared by passing water through an ultra-pure purification system.

1.2 Synthesis of $\text{ZnIr}(\text{OH})_6$ NSs. Typically, 20.4 mg $\text{H}_2\text{IrCl}_6 \cdot \text{H}_2\text{O}$ was dissolved in 10 mL 0.1 M KOH solution for 12 h, followed by adding 6.8 mg ZnCl_2 under ultrasonication and then kept undisturbed for 12 h at room temperature. The resulting precipitation was washed with deionized water by three times and dried at 80 °C in an oven for 12 h.

1.3 Synthesis of $\text{ZnIr}(\text{OH})_6$ NSs/C and *d*- $\text{ZnIr}(\text{OH})_6$ NSs/C. 6 mg $\text{ZnIr}(\text{OH})_6$ NSs was loaded on 10 mg carbon powder under ultrasonication to obtain $\text{ZnIr}(\text{OH})_6$ NSs/C. *d*- $\text{ZnIr}(\text{OH})_6$ NSs/C was obtained by calcinating $\text{ZnIr}(\text{OH})_6$ NSs/C in H_2/Ar for 1 h at 200 °C.

1.4 Synthesis of *d*- $\text{ZnIr}(\text{OH})_6$ -150 NPs/C. *d*- $\text{ZnIr}(\text{OH})_6$ -150 °C NPs/C was obtained by calcinating $\text{ZnIr}(\text{OH})_6$ -150 °C NPs/C in H_2/Ar for 1 h at 200 °C.

1.5 Synthesis of ZnIrO_x NSs/C and Ir/ZnO NSs/C. ZnIrO_x NSs/C was obtained by calcinating $\text{ZnIr}(\text{OH})_6$ NSs/C in Ar for 1 h at 200 °C. Ir/ZnO NSs/C was obtained by calcinating $\text{ZnIr}(\text{OH})_6$ NSs/C in H_2/Ar for 1 h at 300 °C.

1.6 Characterization. Low-magnification TEM was acquired on a HITACHI HT7700 transmission electron microscope at an accelerating voltage of 120 kV. High-resolution TEM (HRTEM) and high-angle annular dark-field scanning TEM (HAADF-STEM) were conducted on a FEI Tecnai F20 transmission electron microscope at an acceleration voltage of 200 kV. AFM measurement was performed by using a Nanoscope V Multimode 8 scanning probe microscope from Bruker Corporation. X-ray diffraction (XRD) patterns were collected on a Shimadzu XRD-6000 X-ray diffractometer. Scanning electron microscopy energy-dispersive X-ray spectroscopy (SEM-EDS) spectra were obtained with a HITACHI S-4700 cold field emission scanning electron microscope. TGA measurement was performed on SII TG/DTA 6300 thermogravimetric analyzer over a temperature range from 25 to 500 °C with a heating rate of 5 °C min⁻¹ in Ar atmosphere. Fourier transform infrared spectra were recorded on a ProStar LC240 spectrometer. The concentration of catalysts was further determined by the inductively coupled plasma atomic emission spectroscopy (710-ES, Varian, ICP-AES). X-ray photoelectron spectra were collected with an SSI S-Probe XPS Spectrometer. The carbon peak at 284.6 eV was used as a reference for calibration. The X-ray absorption data at the Ir *L*₃-edge and Zn *K*-edge of the samples were recorded at room temperature in transmission mode using ion chambers at beamline BL14W1 of the Shanghai Synchrotron Radiation Facility (SSRF), China. In situ X-ray diffraction patterns of the catalysts were recorded on a Rigaku D/Max-2500 X-ray diffractometer using Cu *K* α radiation (2θ in the range of 30–90 ° at a scan rate of 20 ° min⁻¹). In situ X-ray diffraction operated at each of temperatures (50, 100, 150, 170, 180, 200, 220, 240, 260, 280, and 300 °C) in H₂/Ar (5 vol. % in Ar) and pure Ar (99.999%), respectively. In situ visible Raman spectra were collected on a laser Raman spectrometer (Renishaw, inVia reflex) using laser wavelength of 532 nm. In situ Raman spectroscopy was performance at each of temperature points (25, 50, 100, 150, 180, 200, 220, 240, 260, 280, and 300 °C) in atmosphere of H₂/Ar (5 vol. % in Ar).

1.7 Electrochemical measurements. The electrochemical measurements were performed by using a CHI 660E workstation (Chenhua, Shanghai) with a three-electrode configuration. All the experiments were carried out at room temperature. Saturated calomel electrode and Graphite rod were used as the reference and counter electrode, respectively. The inks of different electrocatalysts were prepared by sonicating 2 mg catalyst with 0.4 mL isopropanol and 5 μ L Nafion for 20 min. The working electrode was then fabricated by dropping 10 μ L ink onto a glass carbon electrode (GCE) with a geometric area of 0.196 cm² (loading amount of 50 μ g_{Ir} cm⁻², measured by ICP-AES and EDS). The commercial IrO_x ink was prepared by sonicating 2 mg IrO_x with 0.4 mL isopropanol and 5 μ L Nafion for 20 min. The commercial Pt/C ink was prepared by sonicating 2 mg Pt/C with 0.4 mL isopropanol and 5 μ L Nafion for 20 min. 10 μ L ink was dropped onto the GCE for IrO_x or Pt/C. Linear-sweep voltammograms and chronopotentiometry measurements were carried out to study the catalytic activity and stability, respectively.

Before HER testing, *d*-ZnIr(OH)₆ NSs/C experienced an electrochemical treatment at a potential range of 1.05 to 1.6 V (versus RHE) for 150 cycles at 200 mV s⁻¹ and an additional cyclic voltammetry (CV) activation process at 0 to -0.1 V (versus RHE) for 10 cycles at 200 mV s⁻¹ in 1.0 M KOH. The overall water splitting was conducted with a two-electrode system at scan rate of 5 mV s⁻¹. The electrolytes used were 0.5 M H₂SO₄, 1.0 M KOH, 0.05 M H₂SO₄ and 0.1 M KOH. All the polarization curves were 95 % iR corrected.

1.8 Theoretical calculations. DFT calculations were performed using the Perdew-Burke-Ernzerhof (PBE) functional^{1,2} of generalized gradient approximation (GGA) implemented in Vienna Ab-initio Simulation Package (VASP) code.^{3,4} The projector-augmented wave (PAW) method^{5,6} was applied to describe the electron-ion interactions. A kinetic energy cutoff for the plane wave expansions was set to be 520 eV. The method of Methfessel-Paxton (MP) was applied and the width of the smearing was chosen as 0.2 eV. A 3×3 supercell with six atomic layers was used to construct the Ir (111) surface. To construct the IrO₂ (100) surface, a 2×2 supercell with three atomic layers was used. The slabs were all build in inversion symmetry, and both sides of the slab have been relaxed. More than 15 Å of vacuum space was used to avoid the interaction of the adjacent images. For sampling the reciprocal space, *k*-points of Γ -centered 3×3×1 and Γ -centered 2×4×1 were used for Ir (111) surface and IrO₂ (110) surface, respectively. All structures were fully relaxed until the force components were less than 0.03 eV·Å⁻¹.

The calculated electronic energies were converted into free energies by adding zero-point energies and enthalpic and entropic contributions of adsorbates obtained from a harmonic oscillator at 298.15 K (Tables S4 and 5). Free energy corrections for gaseous molecules were obtained from the ideal gas approximation at 101325 Pa and 3167 Pa for H₂ and H₂O, respectively (Table S6). An H₂O pressure of 3167 Pa is the vapor pressure of H₂O at 298.15 K, where the free energy of gaseous H₂O is equal to that of liquid H₂O.

The delta surface energy $\Delta\gamma(U)$ was calculated as a function of potential:⁷

$$\Delta\gamma(U) = \frac{G_{*O_xH_y} - G_* - xG_{H_2O(l)} + (2x - y)G_{H^+(aq)} - (2x - y)eU}{2A}$$

where $G_{(*O_xH_y)}$ is the free energy of the surface with adsorbed water products (*H, *OH, *OH or *H₂O adsorption), U is the applied potential, e is the electron charge, and A is the surface area of slab. The electrode potential is parametrized within the computational hydrogen electrode scheme and the free energy of the aqueous phase proton, $G_{(H^+(aq))}$ is linked to the pH-independent reversible hydrogen electrode V_{RHE} .

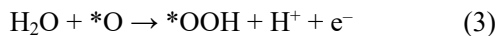
The adsorption free energy for hydrogen under standard conditions ($U = 0$ V) is defined as:⁸

$$\Delta G_H = \Delta E_H + \Delta ZPE - T\Delta S$$

where the ΔE_H is the adsorption energy of H species on the surface from DFT calculations. ΔZPE and $T\Delta S$ are the changes in the zero-point energy and the entropic contribution, respectively.

The reaction mechanism of the oxidation of water involving four sequential proton-coupled electron transfer steps:⁹

11



where * represents the bare catalyst and *OH, *O, and *OOH denote different adsorbed intermediates. For each individual step, the Gibbs free energy ΔG_i ($i = 1, 2, 3$ and 4) under standard conditions ($U = 0$ V) can be calculated using the expression:

$$\Delta G_i = \Delta E + \Delta \text{ZPE} - T\Delta S$$

where ΔE is the total energy difference between the reactant and product molecules in the reactions (Eq. 1–4). ΔZPE and $T\Delta S$ are the changes in the zero-point energy and the entropic contribution, respectively. Thus, based on the above free energy results, the thermodynamic overpotential η^{OER} for a given electrocatalyst can be determined using:

$$G^{\text{OER}} = \max\{\Delta G_1, \Delta G_2, \Delta G_3, \Delta G_4\}$$

$$\eta^{\text{OER}} = G^{\text{OER}}/e - 1.23 \text{ V}$$

where ΔG_1 , ΔG_2 , ΔG_3 and ΔG_4 are the Gibbs free energy for the elementary OER steps.

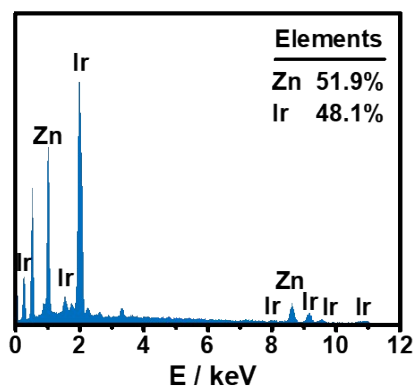


Figure S1. Elemental ratio of $\text{ZnIr}(\text{OH})_6$ NSs. The SEM-EDS spectrum of $\text{ZnIr}(\text{OH})_6$ NSs.

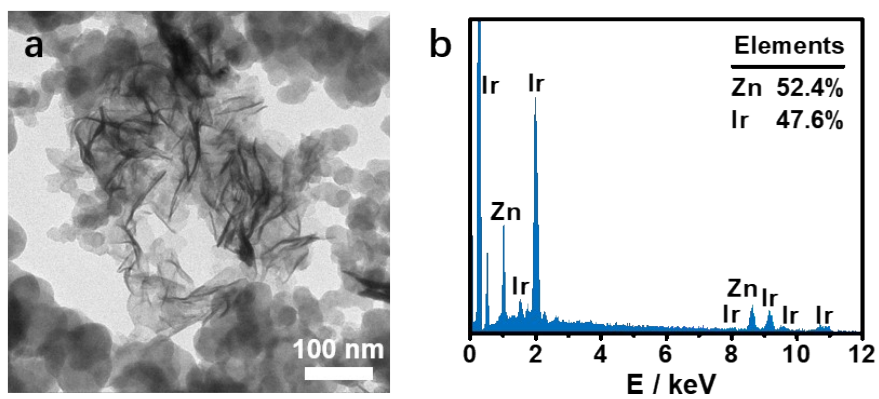


Figure S2. Characterizations of ZnIr(OH)_6 NSs/C. (a) TEM images and (b) EDS profile.

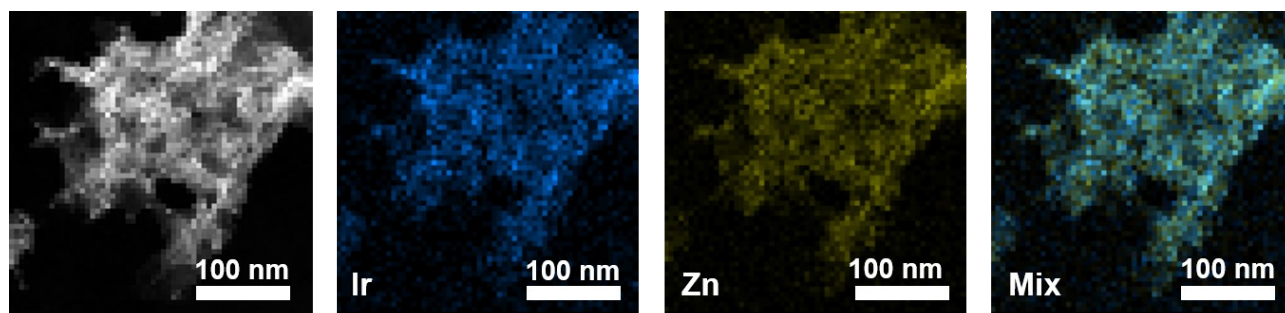


Figure S3. The element mapping of *d*-ZnIr(OH)₆ NSs.

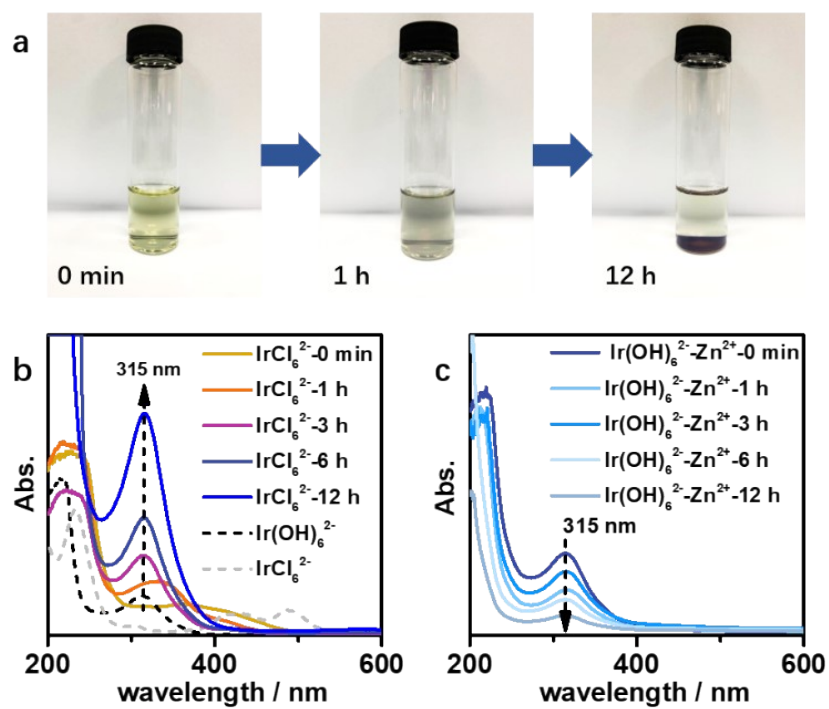


Figure S4. (a) The real pictures during the growth of ZnIr(OH)₆ NSs. UV-visible spectra after H₂IrCl₆ addition (b) and ZnCl₂ (c).

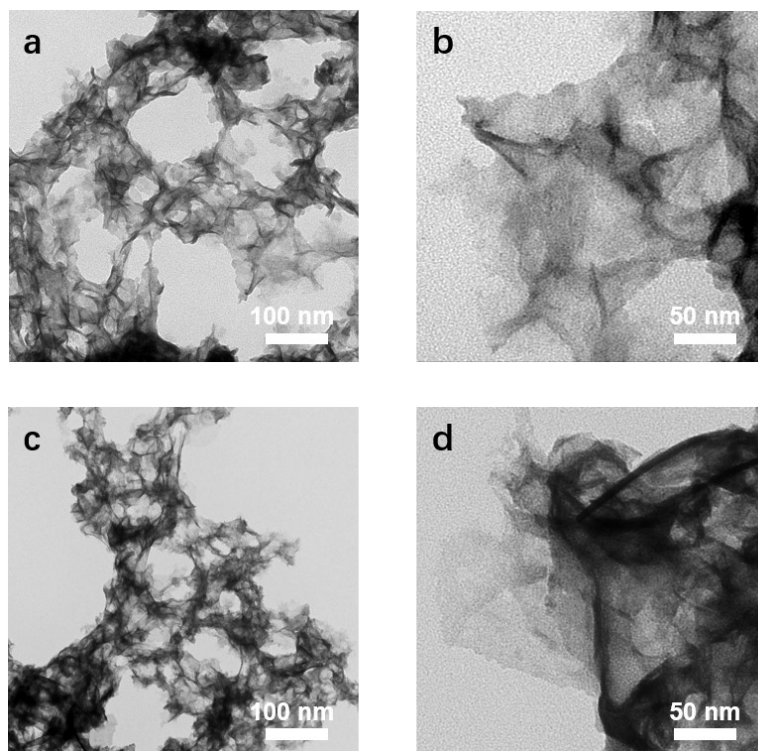


Figure S5. TEM images of $\text{ZnIr}(\text{OH})_6$ collected at different growth times. The products were collected after (a, b) 30 min and (c, d) 6 h.

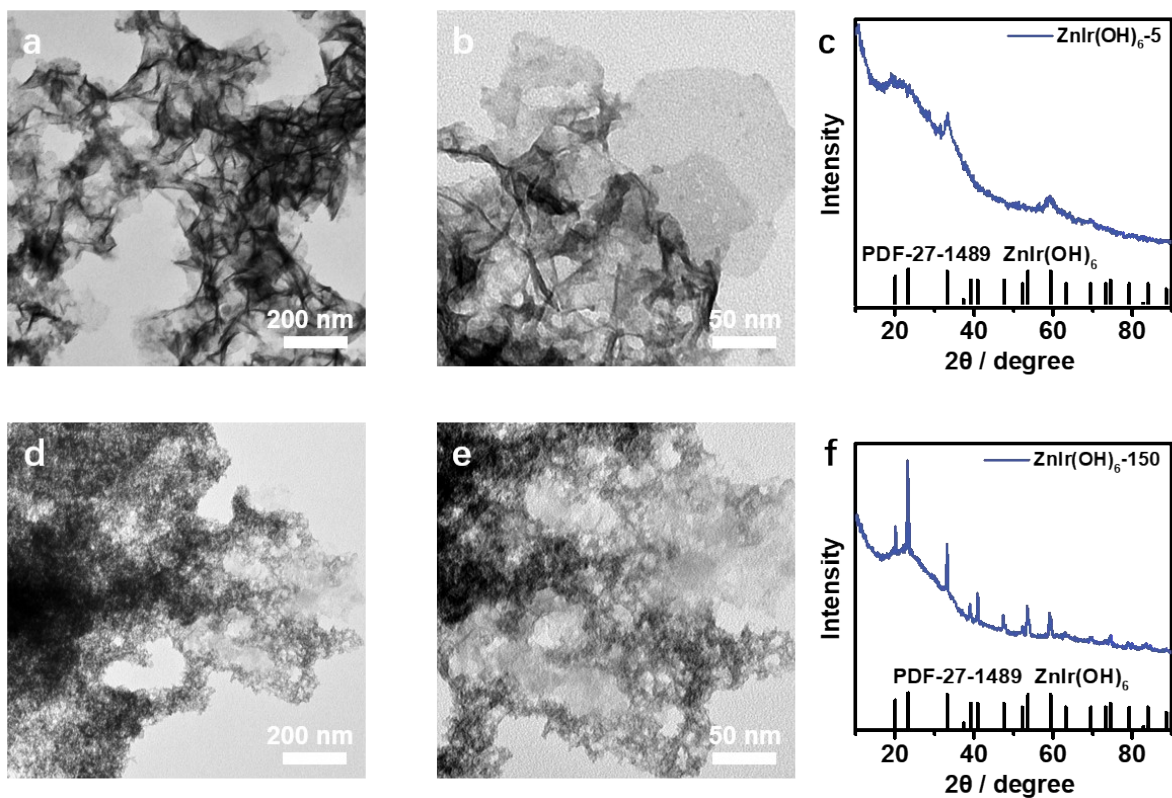


Figure S6. Characterizations of ZnIr(OH)₆ obtained at different temperatures. (a, b) TEM images and (c) XRD pattern of ZnIr(OH)₆ collected at 5 °C. (d, e) TEM images and (f) XRD pattern of ZnIr(OH)₆ collected at 150 °C (named as ZnIr(OH)₆-150 NPs).

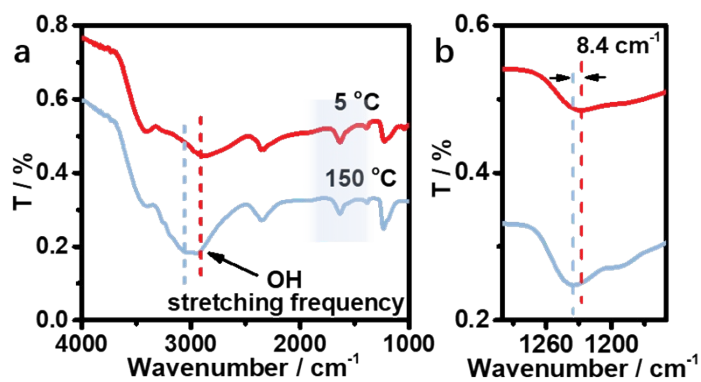


Figure S7. IR spectrum of ZnIr(OH)₆. (a) The peak of OH stretching vibration was labeled in IR spectra. (b) The enlarged peak of Ir-OH in IR spectra.

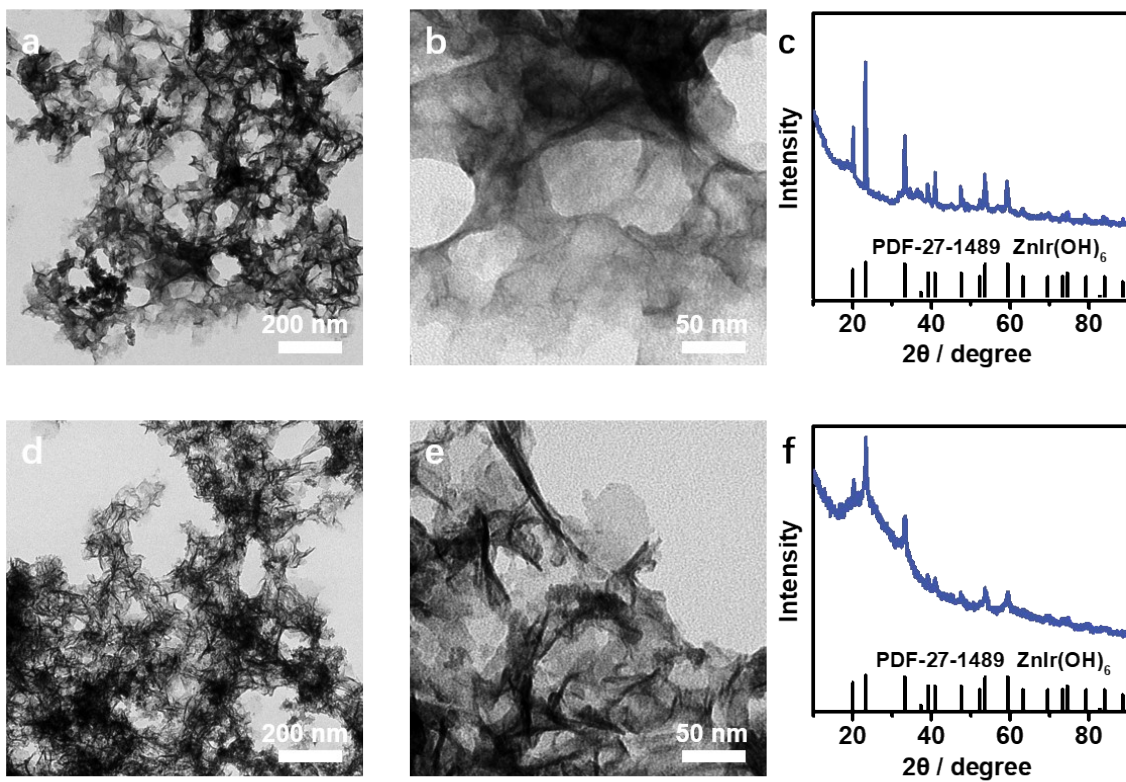


Figure S8. Characterizations of ZnIr(OH)_6 obtained in different bases. (a, b) TEM images and (c) XRD pattern of ZnIr(OH)_6 obtained in NaOH. (d, e) TEM images and (f) XRD pattern of ZnIr(OH)_6 obtained in TMAOH.

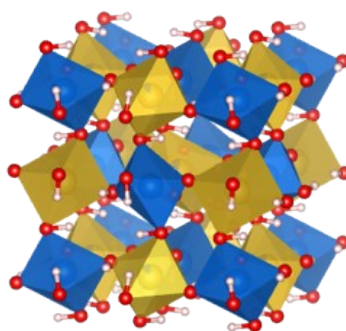


Figure S9. Structural model of $\text{ZnIr}(\text{OH})_6$ NSs.

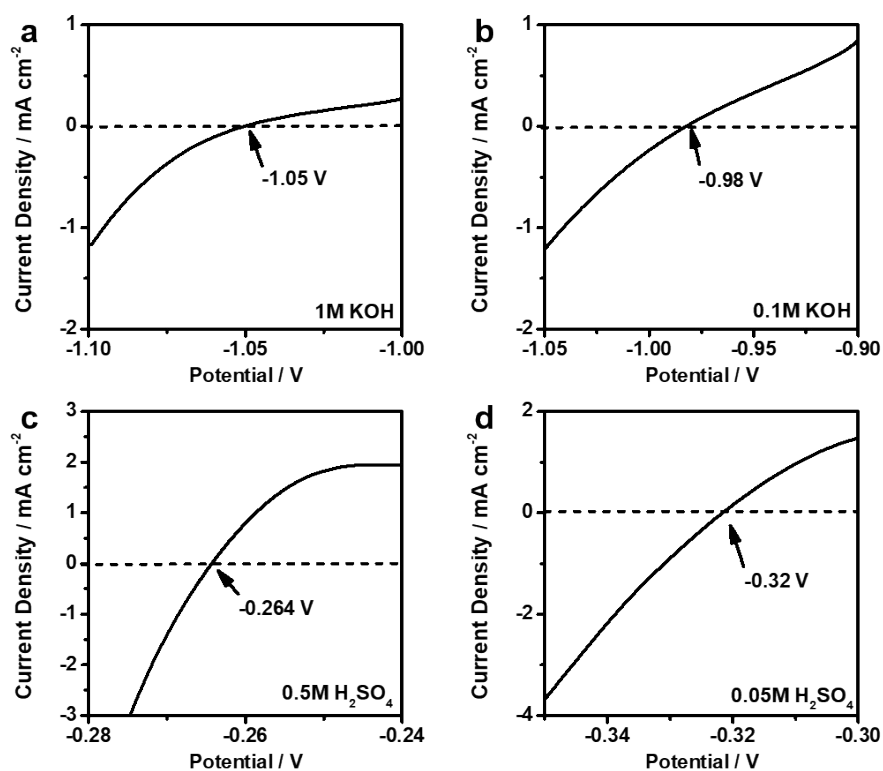


Figure S10. The calibration was performed in a high purity hydrogen-saturated electrolyte with a Pt wire as the working electrode. Linear sweep curves at a scan rate of 5 mV s^{-1} in (a) 1 M KOH, (b) 0.01 M KOH, (c) 0.5 M H_2SO_4 and (d) 0.05 M H_2SO_4 .

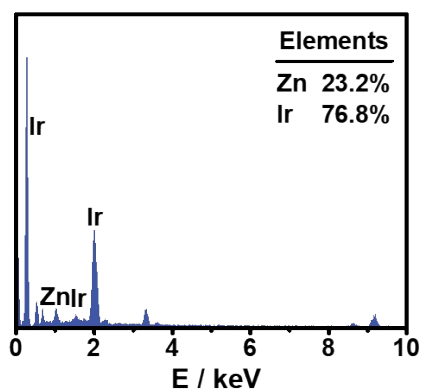


Figure S11. Elemental composition of electrochemically treated d -ZnIr(OH)₆ NSs/C for HER. SEM-EDS spectra of the treated d -ZnIr(OH)₆ NSs/C.

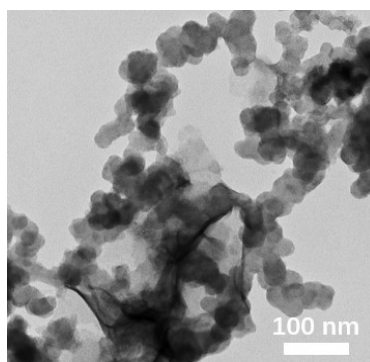


Figure S12. TEM image of CV-activated $d\text{-ZnIr(OH)}_6$ NSs/C for HER. The catalyst experienced a CV activation process from 0 V to -0.1 V (versus RHE) for 10 cycles at 200 mV s^{-1} in 1 M KOH.

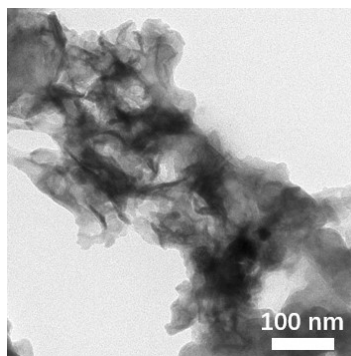


Figure S13. TEM image of CV-activated $d\text{-ZnIr(OH)}_6$ NSs/C for OER. The catalyst experienced a CV activation process from 1.05 V to 1.55 V (versus RHE) for 10 cycles at 200 mV s^{-1} in 1 M KOH.

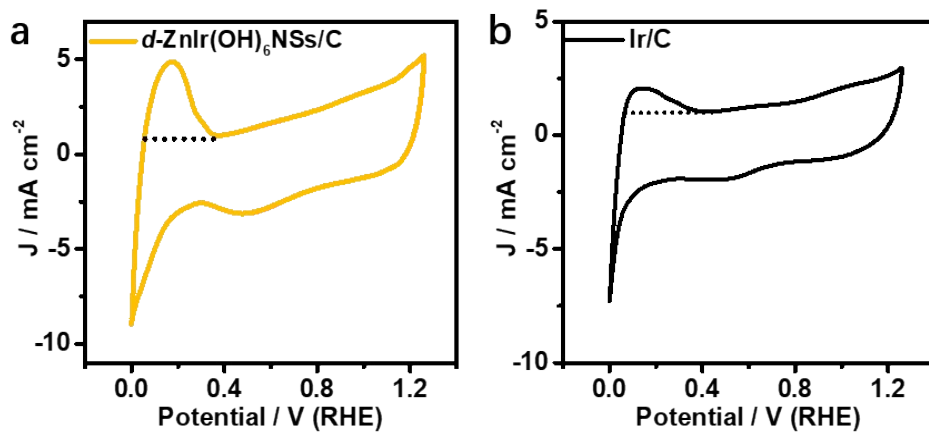


Figure S14. CV curves of (a) $d\text{-ZnIr(OH)}_6\text{NSs/C}$ and (b) Ir/C.

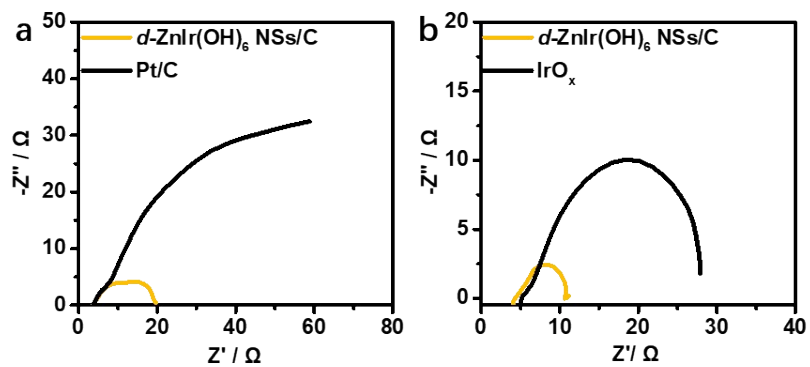


Figure S15. EIS of different catalysts. Initial E at (a) -0.02 V (vs. RHE) for HER and (b) at 1.5 V (vs. RHE) for OER.

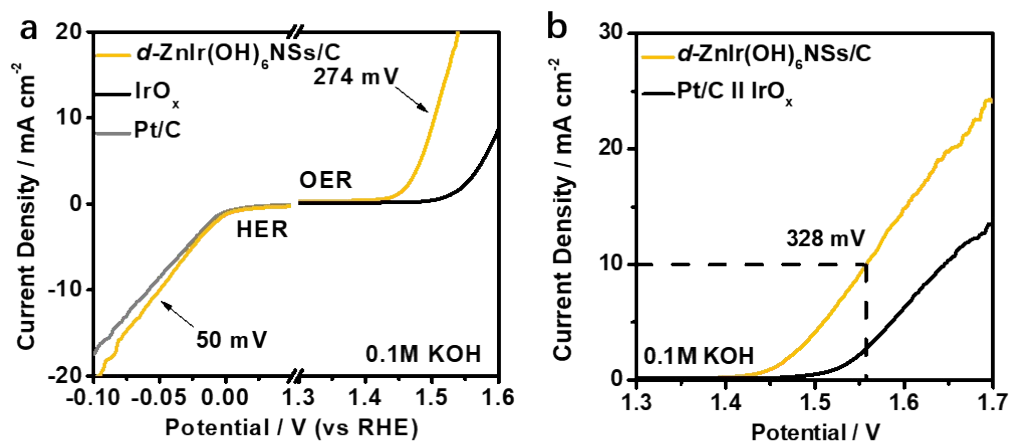


Figure S16. Polarization curves of different catalysts in 0.1 M KOH. Polarization curves for (a) HER and OER, and (b) overall water splitting.

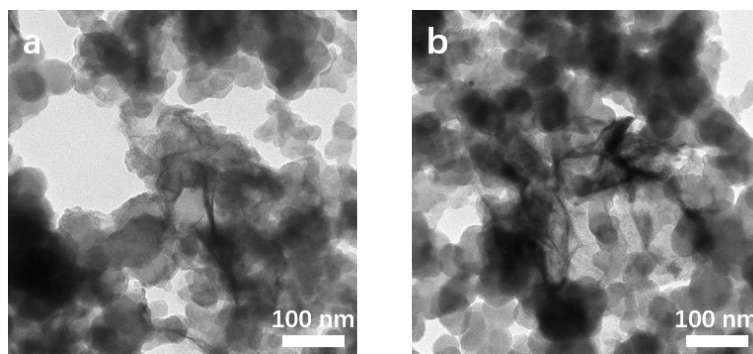


Figure S17. TEM images of spent $d\text{-ZnIr(OH)}_6$ NSs/C in 1 M KOH. TEM image of spent $d\text{-ZnIr(OH)}_6$ NSs/C for (a) HER and (b) OER.

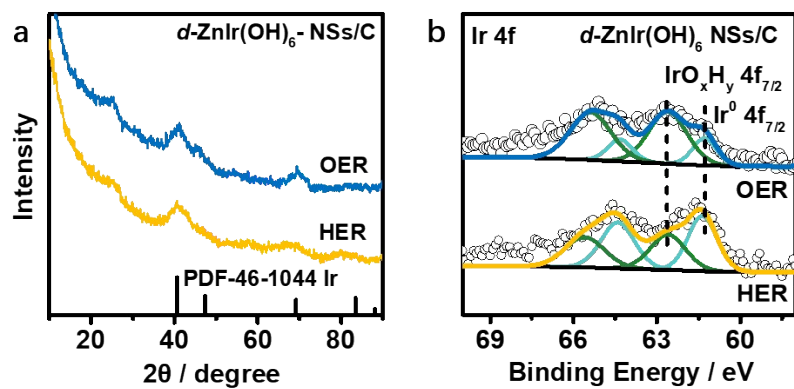


Figure S18. Characterizations of catalysts after overall water splitting in 1 M KOH. (a) XRD pattern and (b) Ir 4f XPS spectra of $d\text{-ZnIr(OH)}_6\text{ NSs/C}$.

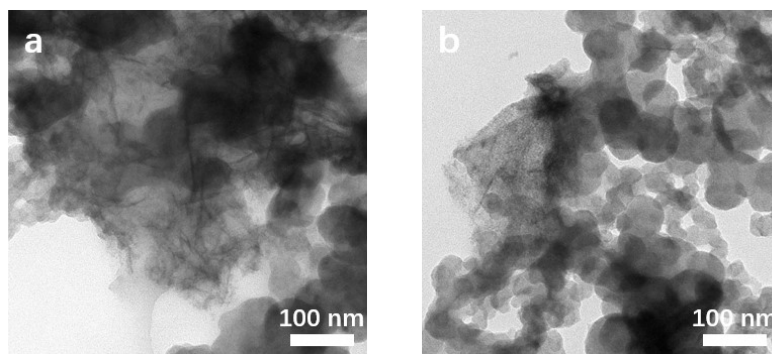


Figure S19. TEM images of spent d -ZnIr(OH)₆ NSs/C in 0.5 M H₂SO₄. TEM image of spent d -ZnIr(OH)₆ NSs/C for (a) HER and (b) OER.

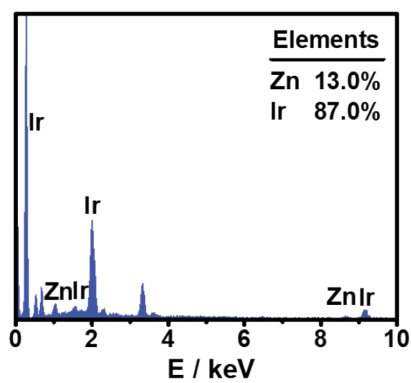


Figure S20. Elemental composition of electrochemically treated d -ZnIr(OH)₆ NSs/C. SEM-EDS spectra of the treated d -ZnIr(OH)₆ NSs/C in 0.5 M H₂SO₄.

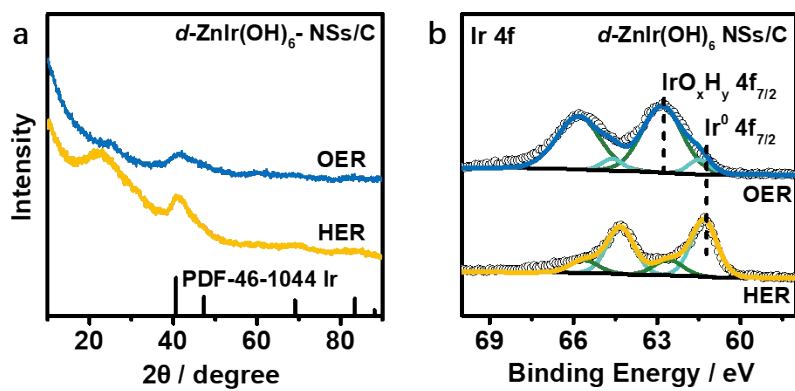


Figure S21. Characterizations of catalysts after overall water splitting in 0.5 M H₂SO₄. (a) XRD pattern and (b) Ir 4f XPS spectra of spent *d*-ZnIr(OH)₆ NSs/C.

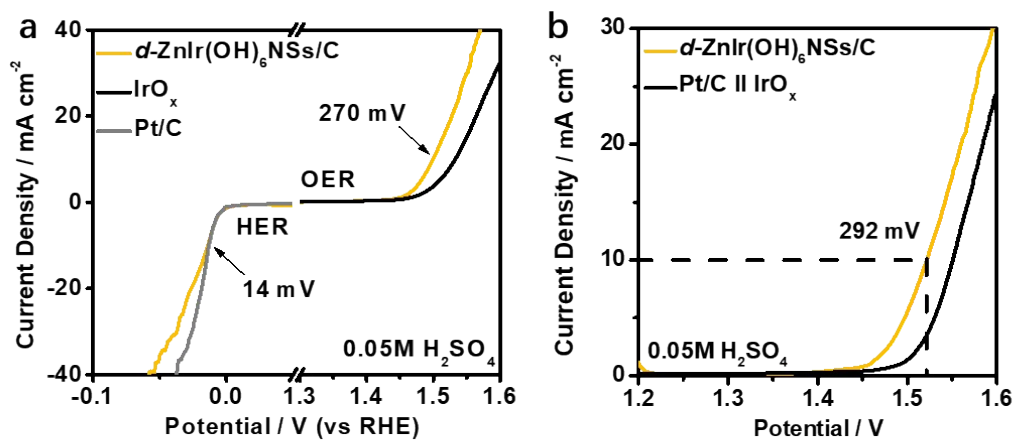


Figure S22. Polarization curves of different catalysts in 0.05 M H₂SO₄. Polarization curves for (a) HER and OER, and (b) overall water splitting.

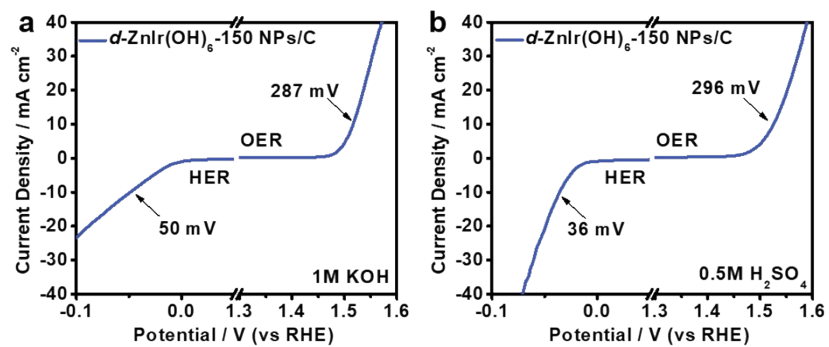


Figure S23. Polarization curves of $d\text{-ZnIr(OH)}_6\text{-150 NPs/C}$ catalysts in (a) 1 M KOH and (b) 0.5 M H_2SO_4 .

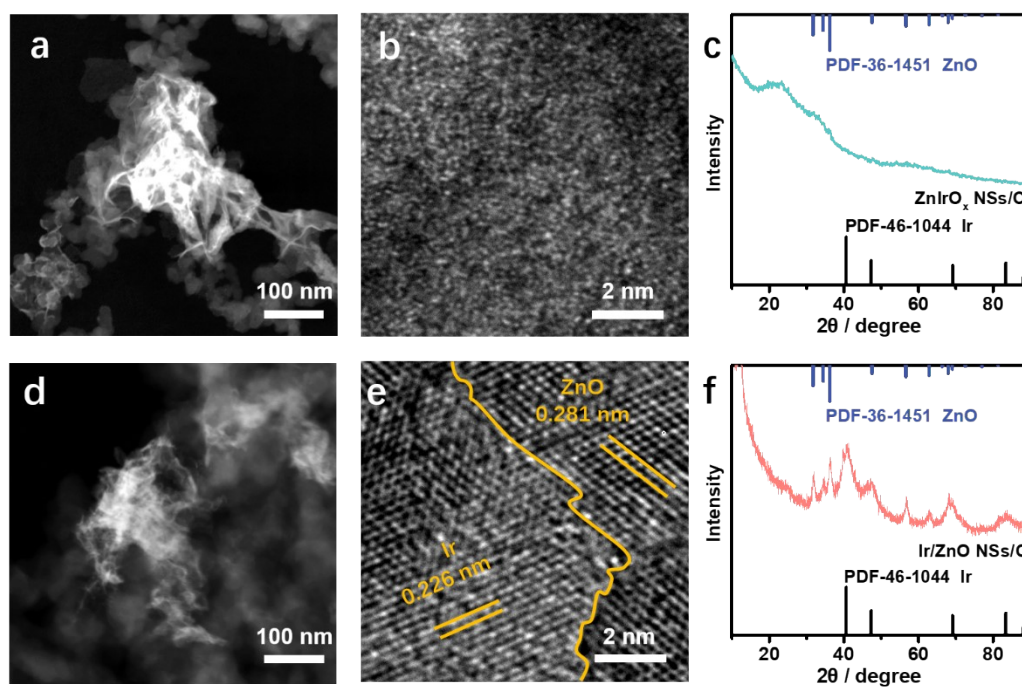


Figure S24. The structural characterizations of different Ir-based NSs. HADDF-STEM images of ZnIrO_x NSs/C (a) and Ir/ZnO NSs/C (d). HRTEM images of ZnIrO_x NSs/C (b) and Ir/ZnO NSs/C (e). XRD patterns of ZnIrO_x NSs/C (c) and Ir/ZnO NSs/C (f).

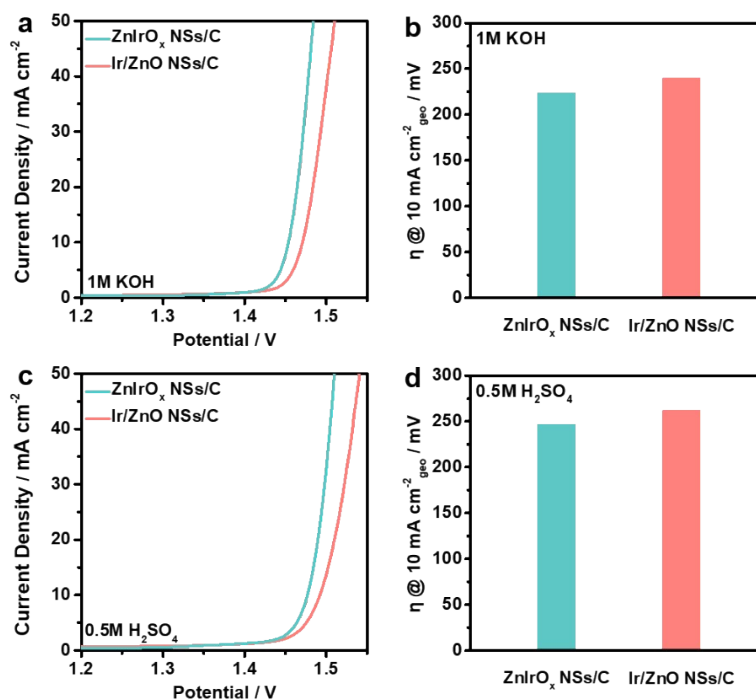


Figure S25. (a, c) OER polarization curves for Ir/ZnO and ZnIrO_x NSs/C in 1.0 M KOH and 0.5 M H₂SO₄. (b, d) Histogram of overpotential for OER over Ir/ZnO NSs/C and ZnIrO_x NSs/C.

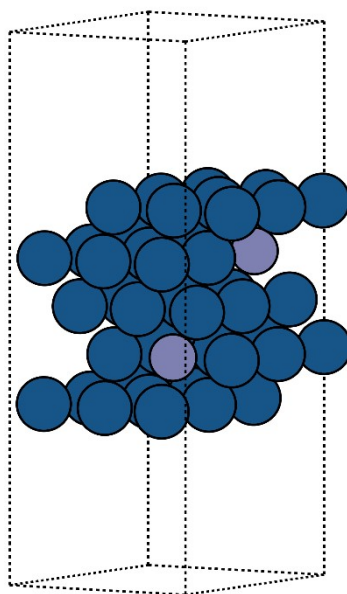


Figure S26. Optimized structure of Zn-Ir surface as the HER catalyst. Blue: Ir, grey: Zn.

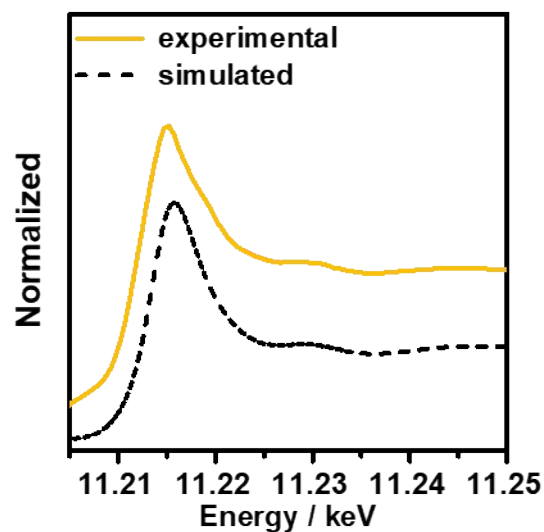


Figure S27. Comparison between the experimental and the simulated L_3 edge XANES spectra based on the DFT model of d -ZnIr(OH)₆ NSs/C. The similar features in the experimental and simulated spectra indicate the applicability of DFT model. The fitting of XANES spectrum at Ir L_3 -edge was simulated on FDMNES¹² based on the cell structure used in DFT calculation. Ir reference was also introduced for comparison. Hubbard energy of 5 eV was used for all the Ir L_3 -edge simulations,¹³ and the Green function employing Muffin-tin potential was applied for the XANES calculations. Besides, normalization was performed with Athena 0.9.26.¹⁴

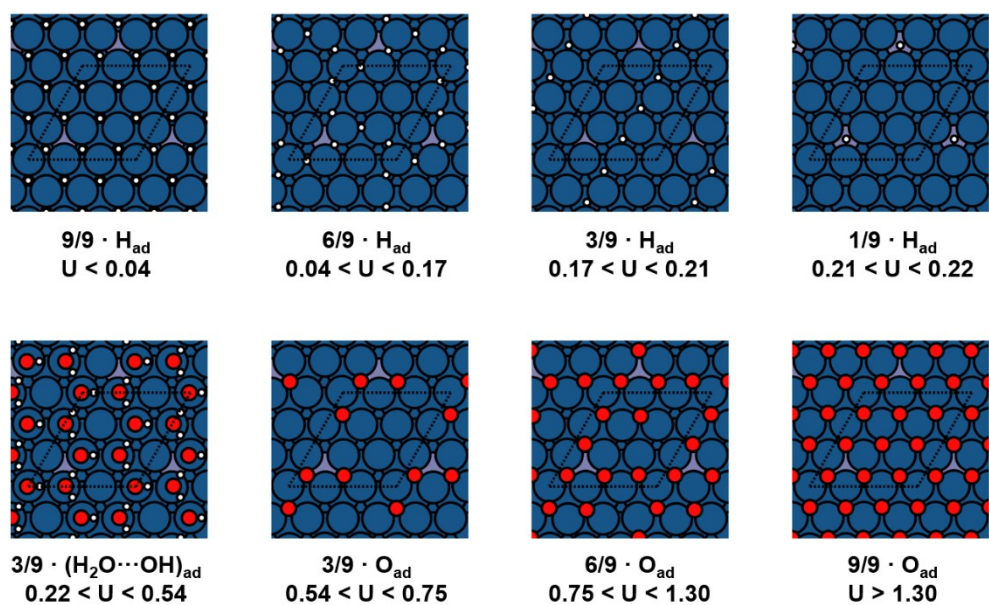


Figure S28. Most stable structures of Zn-Ir catalyst with adsorbed water species (*O, *H, and *OH) under various applied potentials. Blue: Ir, grey: Zn, red: O, and white: H.

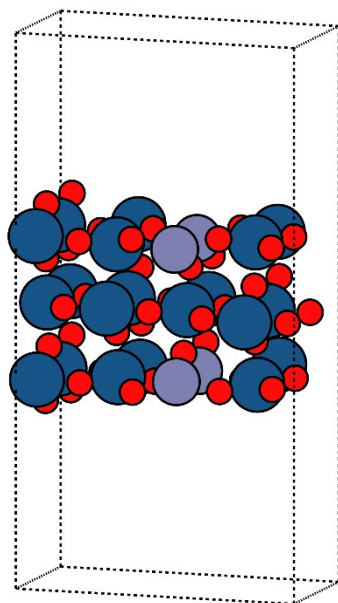


Figure S29. Optimized structure of Zn-IrO_x surface as the OER catalyst. Blue: Ir, grey: Zn, and red: O.

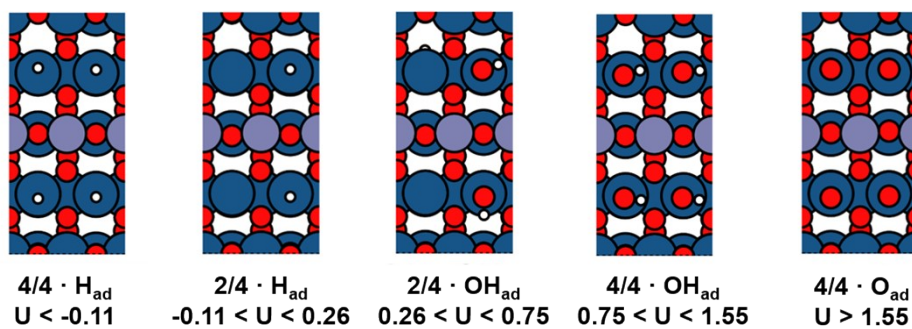


Figure S30. Most stable structures of Zn-IrO_x catalyst with adsorbed water species (*O, *H, and *OH) under various applied potentials. Blue: Ir, grey: Zn, red: O, and white: H.

Table S1. Crystal structure parameters for the EXAFS fitting using the ARTEMIS module of IFEFFIT about Ir powder and *d*-ZnIr(OH)₆.

Sample	Path	CN^a	R / Å	$\sigma^2 / 10^{-3}\text{\AA}^2$	$\Delta E_0 / \text{eV}$	R factor
Ir powder	Ir–Ir	12	2.71±0.01	4.5±0.2	8.81±1.56	0.0085
<i>d</i> -ZnIr(OH) ₆ NSs	Ir–Ir	9.15±1.13	2.67±0.01	7.6±1.0	2.43±1.40	0.0188

^a: CN: coordination number.

Table S2. Comparison between *d*-ZnIr(OH)₆ NSs/C and other reported Ir-based catalysts in alkaline electrolyte.

Reaction	Electrocatalyst	Overpotential/V (at 10 mA cm ⁻²)	Mass loading	Reference
HER	<i>d</i> -ZnIr(OH) ₆ NSs/C	21	250 μg _{cat.} cm ⁻²	This work
	Ir NP/C	28	600 μg _{cat.} cm ⁻²	Adv. Energy Mater. 8 , 1801698 (2018)
	IrP@NC	28	700 μg _{cat.} cm ⁻²	Energy Environ. Sci. 12 , 952–957 (2019)
	IrCo@NC	45	285 μg _{cat.} cm ⁻²	Adv. Mater. 30 , 1705324 (2018)
OER	<i>d</i> -ZnIr(OH) ₆ NSs/C	231	250 μg _{cat.} cm ⁻²	This work
	Ir@Co NSs	273	300 μg _{cat.} cm ⁻²	J. Mater. Chem. A 7 , 8376–8383 (2019)
	Ir NWs	250	570 μg _{cat.} cm ⁻²	ChemCatChem 12 , 1-9 (2020)
Overall water splitting	<i>d</i> -ZnIr(OH) ₆ NSs/C	252	250 μg _{cat.} cm ⁻²	This work
	Li-IrSe	250	3000 μg _{cat.} cm ⁻²	Angew. Chem. Int. Ed. 58 , 14764–14769 (2019)
	PdIr UNWs/WFG	280	200 μg _{cat.} cm ⁻²	Nanoscale 11 , 14561-14568 (2019)
	Ir@Co/NC	373	163 μg _{cat.} cm ⁻²	Angew. Chem. Int. Ed. 58 , 11868–11873 (2019)
	Ir NSs	345	15 μg _{Ir} cm ⁻²	Natl. Sci. Rev. 7 , 1340–1348 (2020)

Table S3. Comparison between *d*-ZnIr(OH)₆ NSs/C and other reported Ir-based catalysts in acidic electrolyte.

Reaction	Electrocatalyst	Overpotential/V (at 10 mA cm ⁻²)	Mass loading	Reference
HER	<i>d</i> -ZnIr(OH) ₆ NSs/C	9	250 μg _{cat.} cm ⁻²	This work
	Ir@CON	13.6	250 μg _{cat.} cm ⁻²	Adv. Mater. 30 , 1805606 (2018)
	Ir/Si NW	22	339 μg _{cat.} cm ⁻²	ACS Nano 13 , 2786–2794 (2019)
	IrCo@NC	24	285 μg _{cat.} cm ⁻²	Adv. Mater. 30 , 1705324 (2018)
OER	<i>d</i> -ZnIr(OH) ₆ NSs/C	252	250 μg _{cat.} cm ⁻²	This work
	Rh ₂₂ Ir ₇₈ /VXC	292	280 μg _{cat.} cm ⁻²	ACS Nano 13 , 13225–13234 (2019)
	Li-IrO _x	270	500 μg _{cat.} cm ⁻²	J. Am. Chem. Soc. 141 , 3014–3023 (2019)
	IrO ₂ /GCN	276	200 μg _{cat.} cm ⁻²	Angew. Chem. Int. Ed. 58 , 12540–12544 (2019)
	6H-SrIrO ₃	248	900 μg _{cat.} cm ⁻²	Nat. Commun. 9 , 5236 (2018)
	<i>d</i> -ZnIr(OH) ₆ NSs/C	278	250 μg _{cat.} cm ⁻²	This work
	Ir-SA@Fe@ NCNT	280	285 μg _{cat.} cm ⁻²	Nano Lett. 20 , 2120–2128 (2020)
Overall water Splitting	Ir-Ag NTs/C	320	13.3 μg _{Ir} cm ⁻²	Nano Energy 56 , 330–337 (2019)
	Ir NSs	356	15 μg _{Ir} cm ⁻²	Natl. Sci. Rev. 7 , 1340–1348 (2020)
	IrNi NFs	370	30 μg _{Ir} cm ⁻²	Small Methods 4 , 1900129 (2019)
	IrCoNi PHNCs	430	10 μg _{Ir} cm ⁻²	Adv. Mater. 29 , 1703798 (2017)
	IrNi NCs	250	12.5 μg _{Ir} cm ⁻²	Adv. Funct. Mater. 27 , 1700886 (2017)
	IrTe ₂ HNSs	360	10 μg _{Ir} cm ⁻²	Adv. Funct. Mater. 30 , 2004375 (2020)
	^a <i>d</i> -ZnIr(OH) ₆ NSs/C	292	250 μg _{cat.} cm ⁻²	This work
	^a IrCo _{0.14} NRs	300	100 μg _{cat.} cm ⁻²	Electrochimica Acta 337 , 135738 (2020)
	^a IrCo _{0.65} NDs	363	90 μg _{cat.} cm ⁻²	ACS Appl. Mater. Interfaces 10 , 24993–24998 (2018)
	^a Ir _{0.5} W _{0.5}	350	60 μg _{cat.} cm ⁻²	Nanoscale, 11 , 8898–8905 (2019)
^a Ir WNWs	390	31 μg _{Ir} cm ⁻²	Nanoscale 10 , 1892–1897 (2018)	

^a: 0.1 M H⁺ electrolyte.

Table S4. Free energy corrections for HER intermediates.

Intermediates	E_{DFT} (eV)	ZPE (eV)	$-TS$ (eV)	G (eV)
*	-429.696	0.000	0.000	-429.696
*H	-433.338	0.158	-0.010	-433.190

Table S5. Free energy corrections for OER intermediates.

Intermediates	E_{DFT} (eV)	ZPE (eV)	$-TS$ (eV)	G (eV)
*	-503.759	0.000	0.000	-503.759
*OH	-513.776	0.361	-0.090	-513.504
*O	-508.585	0.072	-0.063	-508.576
*OOH	-518.384	0.445	-0.141	-518.079

Table S6. Free energy corrections for gas-phase species.

Species	E_{DFT} (eV)	ZPE (eV)	$-TS$ (eV)	G (eV)
H ₂ O	-14.220	0.568	-0.673	-14.325
H ₂	-6.771	0.269	-0.403	-6.905

References

- 1 J. P. Perdew, K. Burke, M. Ernzerhof, *Phys. Rev. Lett.* 1996, **77**, 3865–3868.
- 2 J. P. Perdew, Y. Wang, *Phys. Rev. B* 1992, **45**, 13244–13249.
- 3 G. Kresse, J. Furthmüller, *Phys. Rev. B* 1996, **54**, 11169–11186.
- 4 G. Kresse, J. Furthmüller, *Comput. Mater. Sci.* 1996, **6**, 15–50.
- 5 G. Kresse, J. Hafner, *Phys. Rev. B* 1993, **47**, 558–561.
- 6 P. E. Blöchl, *Phys. Rev. B* 1994, **50**, 17953–17979.
- 7 I. T. McCrum, M. J. Janik, *J. Phys. Chem. C* 2016, **120**, 457–471.
- 8 J. Greeley, T. F. Jaramillo, J. Bonde, I. Chorkendorff, J. K. Nørskov, *Nat. Mater.* 2006, **5**, 909–913.
- 9 J. Rossmeisl, A. Logadottir, J. K. Nørskov, *Chem. Phys.* 2005, **319**, 178–184.
- 10 J. Rossmeisl, Z. W. Qu, H. Zhu, G. J. Kroes, J. K. Nørskov, *J. Electroanalytical Chem.* 2007, **607**, 83–89.
- 11 I. C. Man, H. Y. Su, F. Calle-Vallejo, H. A. Hansen, J. I. Martínez, N. G. Inoglu, J. Kitchin, T. F. Jaramillo, J. K. Nørskov, J. Rossmeisl, *ChemCatChem* 2011, **3**, 1159–1165.
- 12 O. Bunau, Y. Joly, *J. Phys. Condens. Matter.* 2009, **21**, 345501.
- 13 I. Schnell, G. Czycholl, R. C. Albers, *Phys. Rev. B* 2002, **65**, 075103.
- 14 B. Ravel, M. Newville, *J. Synchrotron Radiat.* 2005, **12**, 537–541.